J Nanopart Res (2014) 16:2588
DOI 10.1007/s11051-014-2588-7

RESEARCH PAPER

Copper nanoparticles synthesized by thermal decomposition in liquid phase: the influence of capping ligands on the synthesis and bactericidal activity

Fernando B. Effenberger · Marcos A. Sulca · M. Teresa Machini · Ricardo A. Couto · Pedro K. Kiyohara · Giovanna Machado · Liane M. Rossi

Received: 1 July 2014 / Accepted: 24 July 2014 / Published online: 22 October 2014

Abstract We explored here the synthesis of copper nanoparticles (CuNPs) by thermal decomposition of copper(II) acetate in diphenyl ether in the presence of different capping ligands. To look for any specific role in thermal decomposition, we performed reactions in the presence of oleic acid, oleylamine, and 1,2-octanediol, or in the presence of different combinations of these capping ligands, or in the absence of them. The CuNPs obtained in the presence of oleic acid and oleylamine (in the presence or absence of 1,2-octanediol) were stabilized as Cu(0) NPs, and the "naked" NPs prepared in solvent only easily oxidized to CuO. Therefore, both oleic acid and oleylamine can act as capping ligands to prepare air-stable Cu(0) NPs. The 1,2-alkyldiol is not necessary for metal reduction during the synthesis, but its presence improves size and morphology control. The presence of capping ligands significantly reduced the bactericidal activity exhibited by the Cu NPs against the gram-negative bacteria *Escherichia coli*.

Keywords Copper · Nanoparticles · Thermal decomposition · Oleic acid · Oleylamine · Composite nanoparticle · Bactericidal effect

Guest Editors: Carlos Lodeiro Espiño, José Luis Capelo Martinez

This article is part of the topical collection on Composite Nanoparticles

F. B. Effenberger · R. A. Couto · L. M. Rossi (✉)
Departamento de Química Fundamental, Instituto de Química, Universidade de São Paulo, Av. Prof. Lineu Prestes 748, São Paulo, SP 05508-000, Brazil
e-mail: lrossi@iq.usp.br

Present Address:
F. B. Effenberger
Departamento de Engenharia Química, Centro Universitário da FEI, Av. Humberto Castelo Branco 3972, São Bernardo do Campo, SP 09850-901, Brazil

M. A. Sulca · M. T. Machini
Departamento de Bioquímica, Instituto de Química, Universidade de São Paulo, Av. Prof. Lineu Prestes 748, São Paulo, SP 05508-000, Brazil

Introduction

Particles size and shape are physical attributes that directly influence the physical and chemical properties

P. K. Kiyohara
Instituto de Física, Universidade de São Paulo, CP 66318, São Paulo, SP 05315-970, Brazil

G. Machado
Centro de Tecnologias Estratégicas do Nordeste (CETENE), Av. Luiz Freire 01, Cidade Universitária, Recife, PE 50740-540, Brazil

that are unique to the nanoscale. Therefore, the precise control of the size and shape of nanomaterials, which can be achieved by solution-phase synthesis, is currently a major goal in nanoscience (Wang et al. 2005; Yin and Alivisatos 2005). Catalytic (Kent et al. 2014; Nagaraju et al. 2013; Roucoux et al. 2002), magnetic (Huber 2005; Lu et al. 2007), and optical (Alivisatos 1996; Daniel and Astruc 2004) properties, for example, can in principle be tailored by synthesis design.

The synthesis of nanoparticles (NPs) by thermal decomposition of suitable metal precursors in liquid phase has received attention as a reliable synthetic route to prepare metal NPs of controlled size and shape (Bao et al. 2007; Hiramatsu and Osterloh 2004; Sun et al. 2000; Sun and Zeng 2002). This method potentially offers control of morphological parameters that are not easily achieved by other methods (Lima Jr et al. 2009; Wang et al. 2007). The NPs are synthesized by solution-phase reduction of the metal precursor in the presence of capping ligands and reducing agents. Typical synthetic protocols make use of metal complexes, for example, $M^{x+}(acac)_x$ (M = Fe, Pt, etc.), $Fe(CO)_5$, and others; oleylamine; oleic acid; a long chain alkyl diol, for example, 1,2-hexadecanediol or 1,2-dodecanediol; and a high boiling point solvent, for example, diphenyl ether (bp 265 °C) or dioctyl ether (bp 285 °C). The reaction mixture is refluxed for the preparation of NPs, and the size can be tuned by a seed growth process (Sun et al. 2000) or by changing the surfactant/metal ratios (Crouse and Barron 2008; Wei et al. 2010). The reaction temperature is also an important parameter to control the reducing rate of metal precursors for preparing NPs of controlled size (Xu et al. 2009).

The synthesis of Cu NPs of different sizes was demonstrated by thermally activated coalescence of small-sized particles to form larger-sized particles by desorption of capping molecules, coalescence of nanocrystal seeds, and re-encapsulation of the larger-sized particles (Liu et al. 2007). Higher temperature gives larger average particle size, because desorption of the capping ligands is favored (Mott et al. 2009), which increases coalescence and growth of NPs. In addition, NPs exhibit depressed melting points when compared with their bulk counterparts, which is another important factor for interparticle coalescence and growth (Liu et al. 2007; Mott et al. 2007; Xu et al. 2009). For example, Cu NP with a diameter below 4 nm is theoretically expected to exhibit a melting point below 200 °C (Lisiecki et al. 2000; Mott et al. 2007; Zhu et al. 2005).

While much of the research on the use of thermal decomposition methods has focused on preparing different metal nanoparticles with narrow particle size distributions, little progress has been done to understanding the role of the different components added to the reaction mixture. The synthesis of nanoparticles by the thermal decomposition methods occurs in a complex mixture, and the role of each component has not always been clearly established (Borel 1981; Crouse and Barron 2008; Liu et al. 2007; Mott et al. 2007). Frequently, 1,2-hexadecanediol is suggested as the reducing agent, for example in the synthesis of CuNPs by thermal decomposition (Mott et al. 2007). Here, we explore in detail the synthesis of CuNPs in different combinations of oleic acid, oleylamine, and 1,2-octanediol, and also in the absence of them in order to look for any specific role of such components in the thermal decomposition of $Cu(OAc)_2$.

The preparation of CuNPs is difficult partially because of copper's propensity for oxidation (Chen and Sommers 2001; Kawasaki et al. 2011). A key issue is whether CuNPs can be produced and isolated with controlled size, while keeping the oxidation state of the metal as zero. Despite the wide range of approaches employed toward CuNPs, many techniques show either limited size control or are susceptible to oxidation in air under ambient atmospheric conditions (Dhas et al. 1998; Kawasaki et al. 2011; Zhu et al. 2005), which can be a problem for many applications. CuNPs find important applications in many areas of nanotechnology, including catalysis (Mitsudome et al. 2008), chemical sensing (Chen et al. 2011), and conductive inks (Gamerith et al. 2007; Jeong et al. 2008; Lee et al. 2008; Woo et al. 2008) for inkjet printing technology for the fabrication of electronic components. Despite the antibacterial properties of copper are well recognized (Avery et al. 1996), very little is known about the properties of copper nanoparticles, even though they are potential candidates for the controlled release of copper ions. It has been reported that the antimicrobial activity correlates to the nanoparticle loading that provides the controlled release of copper species (Cioffi et al. 2005). Potential applications include the preparation of antibacterial paints or coatings, where a controlled ion release through a chosen stabilizing shell or

polymeric matrix can be advantageous compared to the use of free copper ions or complexes.

Materials and methods

Synthesis of copper nanoparticles

CuNPs were obtained by adding 2 mmol of $Cu(OAc)_2$ into 20 mL of diphenyl ether with 2 mmol of oleylamine, 2 mmol of oleic acid, and 10 mmol of 1,2-octanediol. The solution was refluxed for 2 h, and the color changed from blue/green to red as the reaction proceeded. After cooling to room temperature, ethanol (100 mL) was added to precipitate the solid, which was separated by centrifugation. Then, the solid was redissolved in 5 mL of toluene and precipitated again with 100 mL of ethanol. After this washing step, the product was isolated as a solid or redissolved in toluene. This sample was named CuNPs_1.

Modifications of the procedure above were made to obtain CuNPs prepared by decomposition of $Cu(OAc)_2$ in diphenyl ether in various reaction conditions: CuNPs_2 were prepared in solvent only (no additives were added); CuNPs_3 were prepared in diphenyl ether and oleic acid; CuNPs_4 were prepared in diphenyl ether and oleylamine; and CuNPs_5 were prepared in diphenyl ether, oleic acid, and oleylamine.

Characterization methods

The nanoparticles' morphology was obtained by transmission electron microscopy (TEM) on a Philips CM 200 operating at accelerating voltage of 200 kV. The samples for TEM were prepared by placing a drop of the nanoparticles toluene solution on a Holey Carbon copper grid. The phase structures of nanoparticles were characterized by X-ray diffraction (XRD). For the XRD analysis, the nanoparticles were isolated as a fine powder and placed in the sample holder. The XRD experiments were carried out on a Rigaku-Denki powder diffractometer equipped with a curved graphite crystal using Cu Kα radiation $\lambda = 1.5418$ Å. The diffraction data were collected at room temperature in a Bragg–Brentano θ–2θ geometry with scan range between 10 and 100°. The diffractograms were obtained with a constant step, $\Delta 2\theta = 0.02$. The indexation of Bragg reflections was obtained by a pseudo-Voigt profile fitting using the FULLPROF code (Schmid 1992). Samples analyzed under oxygen-free conditions were prepared in a glovebox and covered with Kapton tape. UV–Vis analysis was carried out with a Shimadzu UV1800 spectrometer with a 1-cm quartz cuvette. Samples of each synthesis performed were subjected to thermal decomposition by means of thermogravimetric/mass spectrometry (TG/MS) using a NETZSCH STA 409 PC LUXX connected to a NETZSCH Q MS 403 C—quadrupole mass spectrometer. Nitrogen purge gas was used with a flow rate of 50 mL min^{-1}. The samples were heated from 30 to 300 °C at a heating rate of 10 °C min^{-1}.

Antibacterial activity tests

The oleic-acid coated Cu NPs (CuNPs_1) and "naked" CuO NPs (CuNPs_2) were tested against *Escherichia coli* ATCC 25922 based on the method reported by Raffi et al. (2010) and using free copper(II) ions as positive control. The assays were done with (i) stock solution of $CuSO_4$. 5 H_2O in sterilized deionized water diluted to 50 mL with Luria–Bertani (LB) Broth, pH 7.0, to reach concentrations of 0, 20, 40, 60, 80, 100, 150, and 200 μg mL^{-1}; and (ii) dispersion of CuNPs_1 or CuNPs_2 in sterilized deionized water obtained by ultra sonication and equally diluted to give 50 (2.5 mg/50 mL), 100 (5.0 mg/50 mL), 200 (10.0 mg/50 mL), 400 (20.0 mg/50 mL), and 600 (30.0 mg/50 mL) μg mL^{-1}. To each flask with specific concentration of free copper(II) ions or copper NPs, 10^5 colony forming units/mL (CFU mL^{-1}) of fresh bacterial suspension was added. The resulting solution or suspension was incubated at 37 °C for 12 h and 160 rpm on orbital shaking incubator. Bacterial growth monitored each hour by optical density was recorded in a spectrophotometer (UV-1601PC, Shimadzu, Kyoto, Japan) at 600 nm, to obtain the minimal inhibitory concentration (MIC) of copper(II) ions, CuNPs_1, or CuNPs_2. After 6 h of bacteria growth, an aliquot was taken for counting the cells and spreading them onto LB agar plates to observe cells growth at 37 °C for 18–24 h. Plates with 30–300 colonies were the ones taken for cell counting. All experiments were done in triplicate under sterile conditions. The aliquots were taken at 6 h of incubation because the beginning of the stationary phase of microbial growth (maximum number of viable cells) was reached in the conditions employed. The MIC

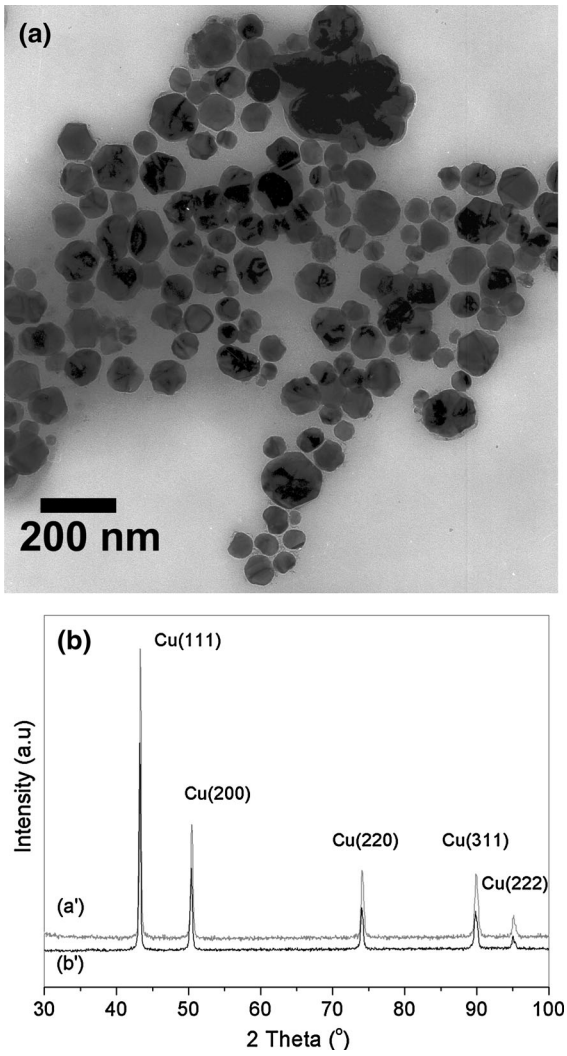

Fig. 1 **a** TEM image of copper particles prepared by the thermal decomposition of $Cu(OAc)_2$ in DPE, OA, OAm, 1,2-OD (CuNPs_1), and **b** XRD pattern of CuNPs_1 (a') under oxygen-free conditions and (b') after exposition to air for 24 h

was defined as the lowest concentration that inhibits the visible microbial growth.

Results and discussion

The synthesis of CuNPs by thermal decomposition was first performed by refluxing a solution of copper(II) acetate, oleylamine (OAm), oleic acid (OA), and 1,2-octanediol (1,2-OD) in the high boiling point solvent diphenyl ether (DPE, bp 265 °C) for 2 h. The color of the mixture changed from blue to red, which is typical of nanosized copper particles. Very stable CuNPs were isolated, redispersed in toluene, and characterized by TEM and XRD as shown in Fig. 1. The TEM image reveals Cu NPs of ca. 60 nm (Fig. 1a).

The organically coated CuNPs are air stable, as can be seen in the XRD diffractogram recorded before and after exposing the sample to air for 24 h (Fig. 1b). The long-range order of the nanoparticles was investigated by XRD on powders samples. The reflections are indexed according to the *F m3 m* symmetry. The XRD pattern confirms the presence of crystalline Cu(0) by the appearance of the most representative Bragg reflections of Cu(0) metal (Fig. 1b), and the most characteristic peaks can be found at scattering angles 2θ of 43.29° (1 1 1), 50.37 ° (2 0 0), 74.25 ° (2 2 0), 89.90 ° (3 1 1) and 95.13 ° (2 2 2).

A theoretical model predicts a decrease in the melting point with decreasing size for copper particles (Matsumoto et al. 2005); however, only NPs smaller than ca. 10 nm have a tendency to melt at the reaction temperature used in this study. Therefore, it is likely that the melting of small-sized NPs and capping ligand adsorption–desorption equilibrium temperature dependence are both processes responsible for particle size growth to ca. 60 nm. Wei et al. (2010) stabilized CuNPs of 34 to 9 nm by varying the excess of oleylamine (9 to 100 times the amount of copper precursor) at lower reaction temperature (155 °C).

The synthesis of CuNPs by thermal decomposition of $Cu(OAc)_2$ in diphenyl ether was studied in more detail by performing the synthesis in different combinations of the components OA and OAm and also in the absence of them. The first reaction was performed by refluxing a solution of $Cu(OAc)_2$ in DPE for 2 h under inert atmosphere (CuNPs_2), and a series of reactions were repeated under similar conditions in the presence of the following additives: OA only (CuNPs_3), OAm only (CuNPs_4), and a mixture of OAm and OA (CuNPs_5). In all syntheses, Cu NPs were always obtained as can be confirmed by TEM and XRD.

TEM images of samples CuNPs_3 to 5 are shown in Fig. 2. In Fig. 2a, the CuNPs_3 synthesized in DPE, and OA exhibited a bimodal particles size distribution. The formation of two different particle sizes is probably due to Ostwald ripening (Murray et al. 2000), and the reaction in this condition needs more time to reach equilibrium. In Fig. 2b, the CuNPs_4

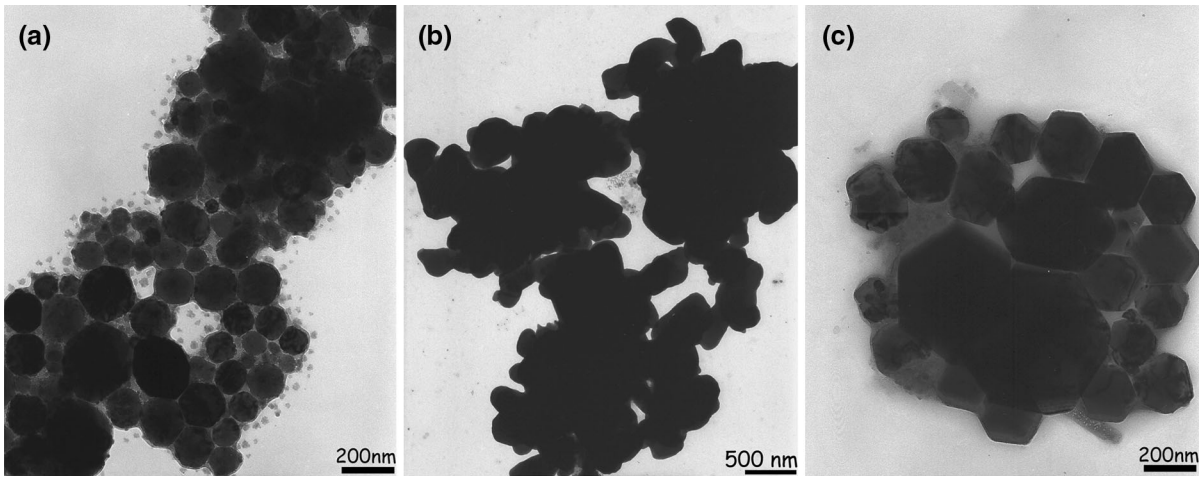

Fig. 2 TEM images of copper particles prepared by the thermal decomposition of $Cu(OAc)_2$ in DPE and **a** OA (CuNPs_3), **b** OAm (CuNPs_4), and **c** a mixture of OAm and OA (CuNPs_5)

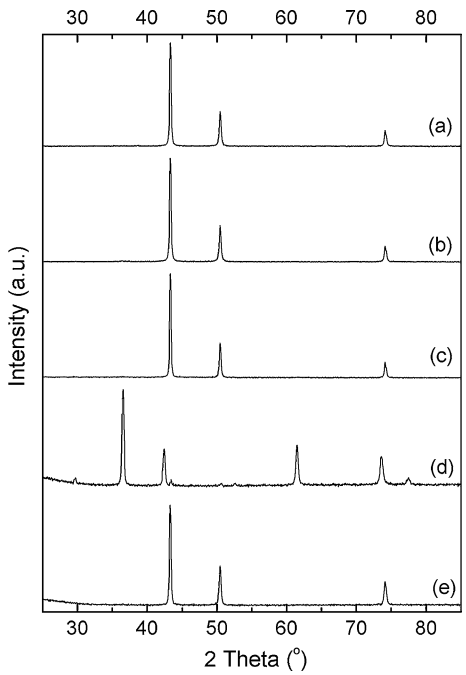

Fig. 3 X-ray diffraction pattern of samples prepared by thermal decomposition of $Cu(AOc)_2$ in DPE: *a* CuNPs_4, *b* CuNPs_5, *c* CuNPs_3, *d* CuNPs_2, and *e* CuNPs_1. All samples were isolated as powders and analyzed in ambient conditions (exposed to air)

synthesized in DPE and OAm exhibited large and unshaped particles. OAm probably acts as a poor capping ligand, and during the particle growth, it does not avoid uncontrolled growth. Otherwise, OAm so as AO prevent nanoparticles oxidation, allowing the isolation of air-stable CuNPs (see discussion of XRD below). Polyhedral faceted particles were obtained in the synthesis in DPE, OA, and OAm in the absence of 1,2-octanediol (CuNPs_5, in Fig. 2c). On the other hand, the synthesis in the presence of 1,2-octanediol, which provides an extra capping "force" on the nanoparticle faces, leads to small and spherical particles (CuNPs_1, Fig. 1a). The XRD patterns of samples CuNPs_3 to 5 are shown in Fig. 3c, a and b, respectively. The position and the relative intensity of all diffraction peaks agree with the diffractogram of the CuNPs obtained by the synthesis in the presence of OA, OAm, and 1,2-OD (CuNPs_1), as shown in Fig. 3e.

The intensities are normalized, and the measured XRD data of Cu NPs were refined by the Rietveld method. In Fig. 3a–c and e, only peaks corresponding to Cu(0) were observed. In the synthesis performed without capping ligands (CuNPs_2), only by refluxing a solution of copper(II) acetate in DPE (see Fig. 3d), the XRD pattern found corresponds to two phases, and the quantifications to each phase were 5 % and 95 % for Cu(0) and CuO, respectively. The CuO phase was indexed with space group *Fm3 m*. The Bragg reflections corresponding to crystalline CuO NPs by Rietveld refinement were observed at 2θ of 36.37°, 42.25°, 61.29°, 73.41°, and 77.26°, which correspond to the indexed planes of copper oxide crystals: (1 1 1), (2 0 0), (2 2 0), (3 1 1), and (2 2 2), respectively, with unit cell parameters of $a = (4.274)$ Å. The Cu(0) phase

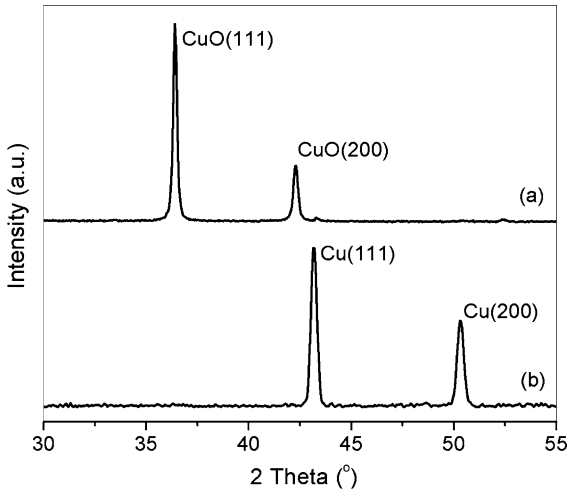

Fig. 4 XRD pattern of samples prepared by thermal decomposition of $Cu(AOc)_2$ in DPE (CuNPs_2) *a* after exposition to air for 24 h and *b* under oxygen-free conditions

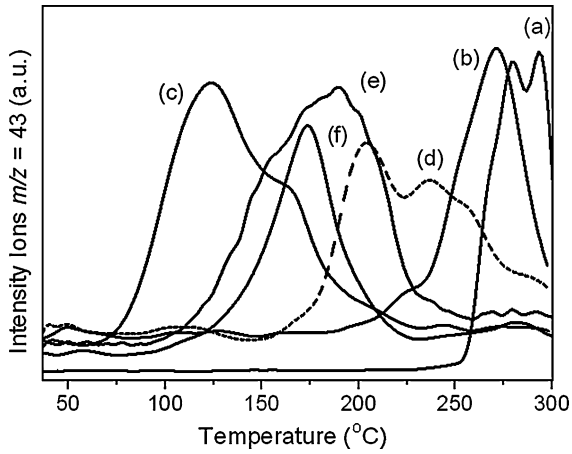

Fig. 5 Mass analysis data of the gas evolved during the thermal analysis (measured by TG-MS) of solutions containing copper(II) acetate: *a* solid, *b* in DPE, *c* in DPE and OA, *d* in DPE and OAm, *e* in DPE, OA, and OAm, and *f* in DPE, OA, OAm, and Diol

presents a structure with space group $Fm\bar{3}\,m$ and 2θ of 43.53° (1 1 1), 50.34° (2 0 0), and 73.25° (2 2 0). The lattice parameter for this sample was determined to be 3.60 Å. It is important to notice that the presence of Cu(0) in the sample is a strong evidence that metal reduction occurred during the synthesis, but in the absence of capping ligands, the "naked" CuNPs oxidized during the workup procedure to CuO. The additives act as capping ligands, but seem to be not needed for metal reduction during the thermal decomposition in liquid phase, neither 1,2-octanediol.

The synthesis of "naked" CuNPs was repeated, and the workup procedure and sample preparation were done under inert atmosphere in a glovebox. The new XRD pattern recorded with the sample protected by Kapton tape is shown in Fig. 4. The sample is constituted of CuNPs with Bragg reflections of Cu(0) metal at scattering angles 2θ of 43.15° (1 1 1) and 50.35° (2 0 0); however, these NPs are not stable in air and oxidize to CuO after removing excess of DPE and exposing it to air. The new XRD pattern recorded after the sample was exposed to air for 24 h as shown in Fig. 4. The sample is constituted of CuO with Bragg reflections of copper oxide at scattering angles 2θ of 36.40° (1 1 1) and 42.30° (2 0 0).

Experiments of thermogravimetry coupled to mass spectrometry (TG-MS) were performed to evaluate the temperature of decomposition of copper(II) acetate in the presence of different additives and DPE upon heating. The ion current of each *m*/*z* value measured in the gas evolved during the thermal analysis is proportional to the evolution rate of the corresponding compound. Figure 5 shows the ion intensity of $m/z = 43$ (CH_3CO^+), which corresponds to the decomposition of the acetate ions in the gas phase (not necessarily the formation of CuNPs as discussed above). It is clearly seen that the additives used in the synthesis can change the temperature of decomposition of copper(II) acetate. Copper(II) acetate decomposes at T > 250 °C (Fig. 5a). In the presence of solvent (DPE), the decomposition temperature decreased about 20 °C (Fig. 5b). In the presence of OA and DPE, the decomposition temperature decreased almost 200 °C to the lower value observed (broad range from 75 to 225 °C) (Fig. 5c). In the presence of OAm and DPE, the decomposition temperature decreased less than 100 °C to a broad decomposition ranging from 160 to 300 °C (Fig. 5d). In the presence of AO, OAm, and DPE, the decomposition temperature decreased to an intermediate value in the range of 100–250 °C (Fig. 5e). The addition of 1,2-octanediol to the mixture of OA, OAm, and DPE narrows the temperature range for decomposition of the copper acetate (Fig. 5f).

The synthesis in the conditions of Fig. 5c was repeated in large scale in order to follow the CuNPs formation as a function of the temperature. The mixture was slowly heated up to reflux, and samples were collected each 10 °C. No metal NPs were

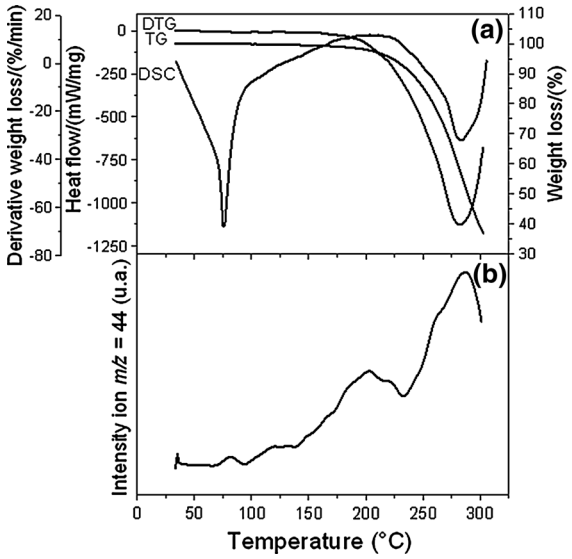

Fig. 6 **a** TG/DTG and DSC obtained in dynamic nitrogen atmosphere (50 mL.min^{-1}) and heating of copper–oleate complex (solid). **b** Mass analysis data of the gas evolved during the thermal analysis (measured by TG-MS) of copper–oleate complex

observed upon heating the mixture at 130 °C for 2 h, and only a green solution ($\lambda_{max} = 680$ nm) was obtained. The presence of CuNPs could be visualized only after reaching temperature higher than 200 °C. Park et al. (2007) in their studies on the thermal decomposition of $Fe(acac)_3$ in the presence of OA reported the formation of the iron–oleate complex at relatively low temperature and its decomposition at a higher temperature to form Fe_3O_4 NPs. We investigated the thermal decomposition behavior of the solid-state copper–oleate precursor prepared by reacting $CuCl_2$ and sodium oleate using thermogravimetric analysis (TG/DTG), differential scanning calorimetry (DSC), and TG-MS (Fig. 6).

The DSC curves revealed two endothermic processes. The first DSC peak at 75 °C can be attributed to the melting of the crystalline $Cu(oleate)_2$, which agrees with the experimental melting point. The second peak at 280 °C matches with the main mass loss process and can be assigned to the decomposition of oleate ligand bound to copper(II) ions. This DSC peak also matches very well with the CO_2 peak ($m/z = 44$) at 287 °C shown in Fig. 6b. The TG/DTG/DSC patterns and the ion $m/z = 44$ intensity curves revealed that the oleate ligand dissociates from the complex precursor after 220 °C by a CO_2 elimination pathway. CO_2 elimination was also observed in the formation of iron oxide NPs from iron–oleate (Park et al. 2004).

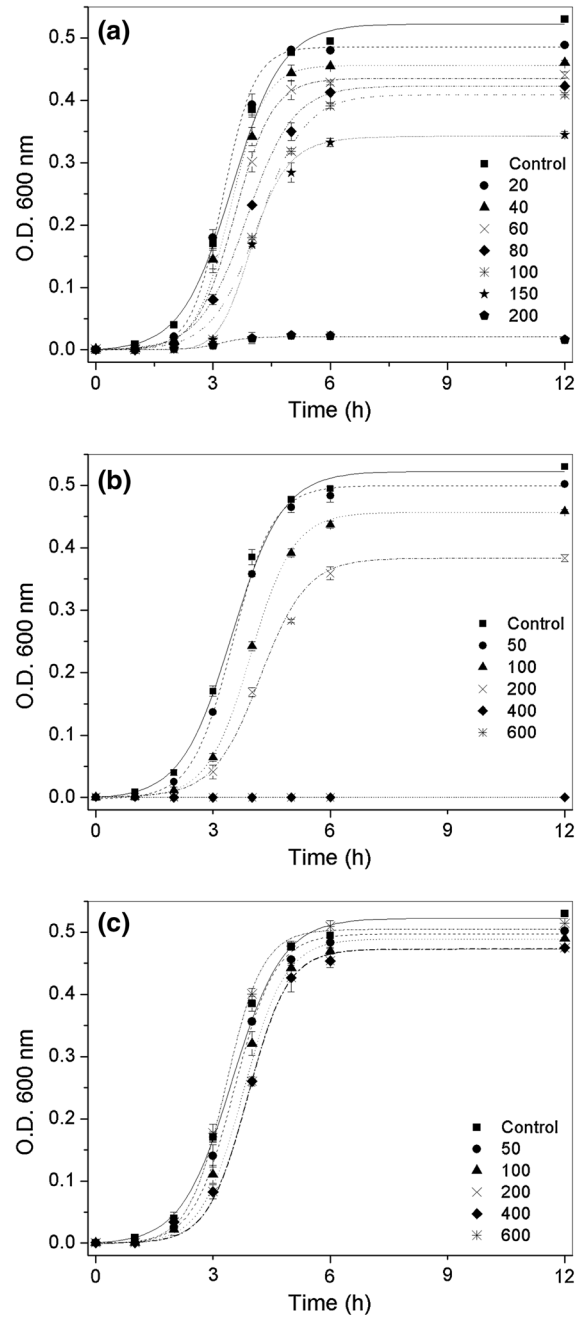

Fig. 7 Curves for time-killing effects on the growth of *Escherichia coli* ATCC 25922 by copper(II) ions (**a**), "naked" CuO NPs (CuNPs_2) (**b**), and oleic-acid coated Cu NPs (CuNPs_1) (**c**) at increasing concentrations in μg mL^{-1}; $n = 3$

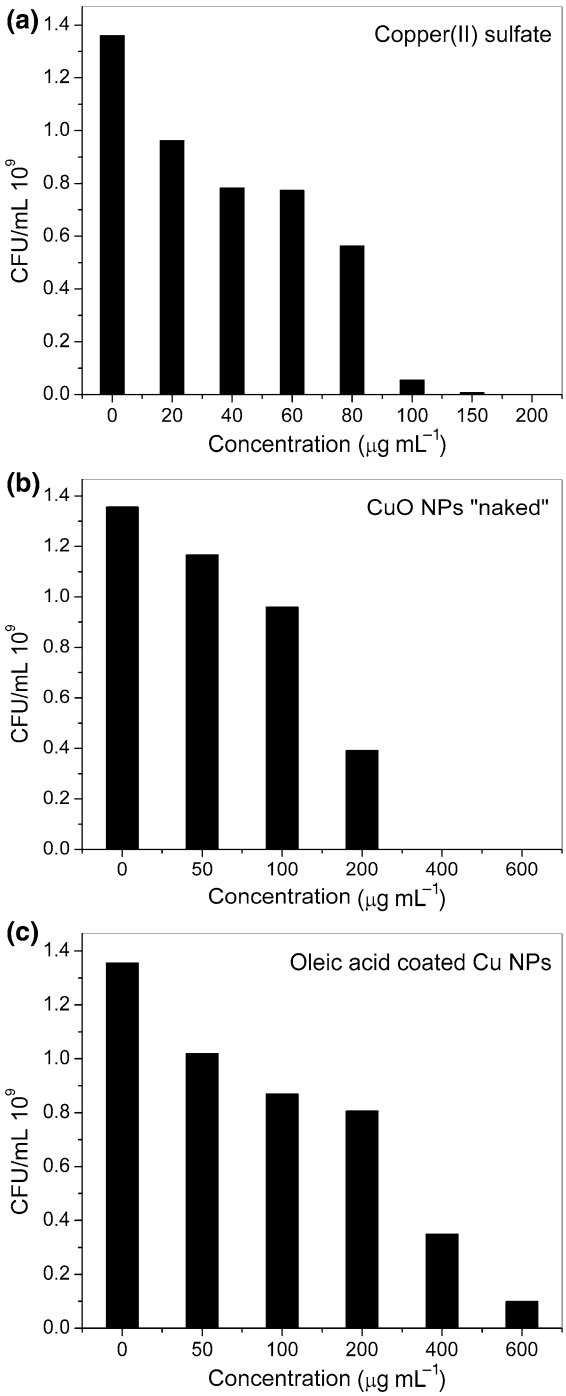

Fig. 8 Antibacterial characterization of copper(II) ions (**a**), "naked" CuO NPs (CuNPs_2) (**b**) and oleic-acid coated Cu NPs (CuNPs_1) (**c**) by colony forming unit (CFU); $n = 3$

As a conclusion, we can suggest that the synthesis of CuNPs by decomposition of copper(II) acetate in the presence of OA occurred in two steps: (i) a ligand exchange process between acetate and oleic acid to form a intermediate copper(II) oleate at lower temperature (the decomposition of acetate starts at 75 °C, Fig. 5c) and (ii) decomposition of this intermediate to form the CuNPs at high temperature (>220 °C, Fig. 6).

To obtain insights into the influence of the presence of capping ligands on the controlled releasing properties and on the bioactivity of the nanoparticles, the oleic-acid coated Cu NPs (sample CuNPs_1) and "naked" CuO NPs (sample CuNPs_2) were tested against the gram-negative bacteria *Escherichia coli*. For that, different concentrations of $CuSO_4$, CuNPs_1, and CuNPs_2 were prepared and tested as described above. As shown in Fig. 7, bacterial cell growth enhances the optical density of liquid nutrient medium in the absence of free copper(II) ions or NPs, but in the presence of increasing concentrations of copper(II) ions, there is a decrease of the optical density evidencing the inhibition of cells growth. The MIC value for free copper(II) ions (200 μg mL^{-1}; Fig. 7a) is lower than that obtained for the "naked" CuO NPs (400 μg mL^{-1}; Fig. 7b), and much lower than obtained for the oleic-acid coated Cu NPs (MIC > 600 μg mL^{-1}, Fig. 7c). The cells counting assay also confirmed this behavior. The results exhibited in Fig. 8a reveal that the higher the amount of copper ions in solution, the lower the number of CFUs, i.e., the stronger the bactericidal effect. The bioactivity of the Cu NPs should be proportional to the concentration of copper ions released to the solution, and not necessarily to the concentration of NPs in the dispersions tested. In summary, the "naked" CuO NPs (Fig. 8b) were able to release significantly more copper than the oleic-acid coated Cu NPs (Fig. 8c) and, therefore, display higher bactericidal effect at lower concentration of NPs.

Conclusions

Copper NPs were obtained by decomposition of copper(II) acetate in diphenyl ether using different combinations of oleylamine, oleic acid, and 1,2-octanediol and also in the absence of such components. It was observed that both oleylamine and oleic acid can act as capping ligands preventing the oxidation of copper NPs. The 1,2-alkyl diol is not necessary for metal reduction during the synthesis, as

usually suggested, but its presence provides size and morphology control. None of the mentioned reagents have a specific role as reducing agent in the synthesis, because CuNPs were isolated from different formulations, even in solvent only. However, in the absence of additives, the "naked" CuNPs oxidize to CuO. Like their noble metal counterparts, the organically protected CuNPs are stable in both solution and dry forms. Moreover, the presence of capping organic ligands, such as oleic acid, not only avoids the oxidation of the Cu NPs, but also modulates their potential biological application.

Acknowledgments The authors are grateful to the Brazilian agencies FAPESP and CNPq for financial support. We also thank Prof. Ana Maria Ferreira (Instituto de Química, Universidade de São Paulo) for TG-MS measurements (FAPESP Grant 05/60596-8). MTM and LMR are members of the NAPCatSinQ-USP.

References

Alivisatos AP (1996) Semiconductor clusters, nanocrystals, and quantum dots. Science 271:933–937

Avery SV, Howlett NG, Radice S (1996) Copper toxicity towards Saccharomyces cerevisiae: dependence on plasma membrane fatty acid composition. Appl Environ Microbiol 62:3960–3966

Bao N, Shen L, Wang Y, Padhan P, Gupta A (2007) A facile thermolysis route to monodisperse ferrite nanocrystals. J Am Chem Soc 129:12374–12375

Borel J-P (1981) Thermodynamical size effect and the structure of metallic clusters. Surf Sci 106:1–9

Chen S, Sommers JM (2001) Alkanethiolate-protected copper nanoparticles: spectroscopy, electrochemistry, and solid-state morphological evolution. J Phys Chem B 105:8816–8820

Chen X, Tian X, Shin I, Yoon J (2011) Fluorescent and luminescent probes for detection of reactive oxygen and nitrogen species. Chem Soc Rev 40:4783–4804

Cioffi N, Torsi L, Ditaranto N, Tantillo G, Ghibelli L, Sabbatini L (2005) Copper nanoparticles/polymer composites with antifungal and bacteriostatic properties. Chem Mater 17:5255–5262

Crouse CA, Barron AR (2008) Reagent control over the size, uniformity, and composition of Co-Fe-O nanoparticles. J Mater Chem 18:4146–4153

Daniel M-C, Astruc D (2004) Gold nanoparticles: assembly, supramolecular chemistry, quantum-size-related properties, and applications toward biology, catalysis, and nanotechnology. Chem Rev 104:293–346

Dhas NA, Raj CP, Gedanken A (1998) Synthesis, characterization, and properties of metallic copper nanoparticles. Chem Mater 10:1446–1452

Gamerith S, Klug A, Scheiber H, Scherf U, Moderegger E, List EJ (2007) Direct ink-jet printing of Ag–Cu nanoparticle and Ag-precursor based electrodes for OFET applications. Adv Funct Mater 17:3111–3118

Hiramatsu H, Osterloh FE (2004) A simple large-scale synthesis of nearly monodisperse gold and silver nanoparticles with adjustable sizes and with exchangeable surfactants. Chem Mater 16:2509–2511

Huber DL (2005) Synthesis, properties, and applications of iron nanoparticles. Small 1:482–501

Jeong S et al (2008) Controlling the thickness of the surface oxide layer on Cu nanoparticles for the fabrication of conductive structures by ink-jet printing. Adv Funct Mater 18:679–686

Kawasaki H, Kosaka Y, Myoujin Y, Narushima T, Yonezawa T, Arakawa R (2011) Microwave-assisted polyol synthesis of copper nanocrystals without using additional protective agents. Chem Commun 47:7740–7742

Kent PD, Mondloch JE, Finke RG (2014) A four-step mechanism for the formation of supported-nanoparticle heterogeneous catalysts in contact with solution: the conversion of Ir(1,5-COD)Cl/γ-Al_2O_3 to Ir(0)($\sim$170)/γ-Al_2O_3. J Am Chem Soc 136:1930–1941

Lee Y, J-r Choi, Lee KJ, Stott NE, Kim D (2008) Large-scale synthesis of copper nanoparticles by chemically controlled reduction for applications of inkjet-printed electronics. Nanotechnology 19:415604

Lima E Jr et al (2009) Single-step chemical synthesis of ferrite hollow nanospheres. Nanotechnology 20:045606

Lisiecki I, Sack-Kongehl H, Weiss K, Urban J, Pileni M-P (2000) Annealing process of anisotropic copper nanocrystals. 1. Cylinders Langmuir 16:8802–8806

Liu X, Atwater M, Wang J, Dai Q, Zou J, Brennan JP, Huo Q (2007) A study on gold nanoparticle synthesis using oleylamine as both reducing agent and protecting ligand. J Nanosci Nanotechnol 7:3126–3133

Lu A-H, Salabas EL, Schüth F (2007) Magnetic nanoparticles: synthesis, protection, functionalization, and application. Angew Chem Int Ed 46:1222–1244

Matsumoto T, Fujii H, Ueda T, Kamai M, Nogi K (2005) Measurement of surface tension of molten copper using the free-fall oscillating drop method. Meas Sci Technol 16:432

Mitsudome T, Mikami Y, Ebata K, Mizugaki T, Jitsukawa K, Kaneda K (2008) Copper nanoparticles on hydrotalcite as a heterogeneous catalyst for oxidant-free dehydrogenation of alcohols. Chem Commun 39:4804–4806

Mott D, Galkowski J, Wang L, Luo J, Zhong C-J (2007) Synthesis of size-controlled and shaped copper nanoparticles. Langmuir 23:5740–5745

Mott D et al (2009) From ultrafine thiolate-capped copper nanoclusters toward copper sulfide nanodiscs: a thermally activated evolution route. Chem Mater 22:261–271

Murray CB, Kagan C, Bawendi M (2000) Synthesis and characterization of monodisperse nanocrystals and close-packed nanocrystal assemblies. Annu Rev Mater Sci 30: 545–610

Nagaraju G, Ebeling G, Gonçalves RV, Teixeira SR, Weibel DE, Dupont J (2013) Controlled growth of TiO2 and TiO2–RGO composite nanoparticles in ionic liquids for enhanced photocatalytic H2 generation. J Mol Catal A: Chem 378: 213–220

Park J et al (2004) Ultra-large-scale syntheses of monodisperse nanocrystals. Nat Mater 3:891–895

Park J, Joo J, Kwon SG, Jang Y, Hyeon T (2007) Synthesis of monodisperse spherical nanocrystals. Angewandte Chemie-Int Ed 46:4630–4660

Raffi M, Mehrwan S, Bhatti TM, Akter JI, Hameed A, Yawar W, Hasan M (2010) Investigations into the antibacterial behavior of copper nanoparticles against *Escherichia coli*. Ann Microbiol 60:75–80

Roucoux A, Schulz J, Patin H (2002) Reduced transition metal colloids: a novel family of reusable catalysts? Chem Rev 102:3757–3778

Schmid G (1992) Large clusters and colloids. Metals in the embryonic state. Chem Rev 92:1709–1727

Sun SH, Zeng H (2002) Size-controlled synthesis of magnetite nanoparticles. J Am Chem Soc 124:8204–8205

Sun SH, Murray CB, Weller D, Folks L, Moser A (2000) Monodisperse FePt nanoparticles and ferromagnetic FePt nanocrystal superlattices. Science 287:1989–1992

Wang X, Zhuang J, Peng Q, Li Y (2005) A general strategy for nanocrystal synthesis. Nature 437:121–124

Wang C, Daimon H, Lee Y, Kim J, Sun S (2007) Synthesis of monodisperse Pt nanocubes and their enhanced catalysis for oxygen reduction. J Am Chem Soc 129:6974–6975

Wei Y, Chen S, Kowalczyk B, Huda S, Gray TP, Grzybowski BA (2010) Synthesis of stable, low-dispersity copper nanoparticles and nanorods and their antifungal and catalytic properties. J Phys Chem C 114:15612–15616

Woo K, Kim D, Kim JS, Lim S, Moon J (2008) Ink-Jet printing of Cu—Ag-based highly conductive tracks on a transparent substrate. Langmuir 25:429–433

Xu Z, Shen C, Hou Y, Gao H, Sun S (2009) Oleylamine as both reducing agent and stabilizer in a facile synthesis of magnetite nanoparticles. Chem Mater 21:1778–1780

Yin Y, Alivisatos AP (2005) Colloidal nanocrystal synthesis and the organic-inorganic interface. Nature 437:664–670

Zhu H, Zhang C, Yin Y (2005) Novel synthesis of copper nanoparticles: influence of the synthesis conditions on the particle size. Nanotechnology 16:3079